

Bio-convective flow of gyrotactic microorganisms in nanofluid through a curved oscillatory channel with Cattaneo–Christov double diffusion theory

Imran M, Naveed M, Rafiq M Y, and Abbas Z

Citation: Chin. Phys. B, 2026, 35 (**1**): 014401. DOI: 10.1088/1674-1056/ade066
http://cpb.iphy.ac.cn; http://iopscience.iop.org/cpb

What follows is a list of articles you may be interested in

Finite element analysis of copper nanoparticles in Boger fluid: Effects of dynamic inter-particle spacing, nanolayer thermal conductivity, nanoparticles diameter, and thermal radiation over a stretching sheet

Qadeer Raza, Xiaodong Wang(王晓东), Tahir Mushtaq, Bagh Ali, and Nehad Ali Shah
Chin. Phys. B, 2025, 34 (**11**): 114402. DOI: 10.1088/1674-1056/addcbc

Cattaneo-Christov heat transfer model for tangent hyperbolic fluid with Thompson-Torian slip and melting effects

Anwar Saeed and Afrah Al-Bossly
Chin. Phys. B, 2025, 34 (**9**): 094404. DOI: 10.1088/1674-1056/add90a

Influences of double diffusion upon radiative flow of thin film Maxwell fluid through a stretching channel

Arshad Khan, Ishtiaq Ali, Musawa Yahya Almusawa, Taza Gul, and Wajdi Alghamdi
Chin. Phys. B, 2023, 32 (**8**): 084401. DOI: 10.1088/1674-1056/acc059

Influences of Marangoni convection and variable magnetic field on hybrid nanofluid thin-film flow past a stretching surface

Noor Wali Khan, Arshad Khan, Muhammad Usman, Taza Gul, Abir Mouldi, and Ameni Brahmia
Chin. Phys. B, 2022, 31 (**6**): 064403. DOI: 10.1088/1674-1056/ac3a5d

Flow and heat transfer of a nanofluid over a hyperbolically stretching sheet

A. Ahmad, S. Asghar, A. Alsaedi
Chin. Phys. B, 2014, 23 (**7**): 074401. DOI: 10.1088/1674-1056/23/7/074401

Bio-convective flow of gyrotactic microorganisms in nanofluid through a curved oscillatory channel with Cattaneo–Christov double diffusion theory

Imran M[1,†], Naveed M[1], Rafiq M Y[2], and Abbas Z[2]

[1] *Department of Mathematics, Division of Science and Technology, University of Education, Lahore* 54770, *Pakistan*
[2] *Department of Mathematics, The Islamia University of Bahawalpur, Bahawalpur* 63100, *Pakistan*

(Received 2 March 2025; revised manuscript received 8 May 2025; accepted manuscript online 4 June 2025)

The present study investigates the flow, heat, and mass transfer analysis in the bioconvection of nanofluid containing motile gyrotactic microorganisms through a semi-porous curved oscillatory channel with a magnetic field. These microorganisms produce density gradients by swimming, which induces macroscopic convection flows in the fluid. This procedure improves the mass and heat transfer, illustrating the interaction between biological activity and fluid dynamics. Furthermore, instead of considering traditional Fourier's and Fick's law the energy and concentration equations are developed by incorporating Cattaneo–Christov double diffusion theory. Moreover, to examine the influence of thermophoresis and Brownian diffusions in the fluid we have adopted the Buongiorno nanofluid model. Due to the oscillation of the surface of the channel, the mathematical development of the considered flow problem is obtained in the form of partial differential equations via the curvilinear coordinate system. The convergent series solution of the governing flow equations is obtained after applying the homotopy analysis method (HAM). The effects of different pertinent flow parameters on velocity, motile microorganism density distribution, concentration, pressure, temperature, and skin friction coefficient are examined and discussed in detail with the help of graphs and tables. It is observed during the current study that the density of microorganisms is enhanced for higher values of Reynolds number, Peclet number, radius of curvature variable, and Lewis number.

Keywords: semi-porous oscillatory curved channel, gyrotactic microorganisms, magnetohydrodynamic, viscous nanofluid, Cattaneo–Christov double diffusion, homotopy analysis method

PACS: 44.05.+e, 44.20.+b, 82.60.Qr, 44.25.+f

DOI: 10.1088/1674-1056/ade066 **CSTR:** 32038.14.CPB.ade066

1. Introduction

The study of numerous boundary layer flow problems in tubes or semi-permeable/permeable channels has fascinated the attention of engineers and scholars over the past few years owing to its extensive range of reasonable applications in biomedical and mechanical manufacturing. Such applications include semi-permeable or permeable pipe development, capillary blood flow, and movement of blood in oxygenators, filter drawing, and blood dialysis in synthetic kidneys. Berman[1] investigated the steady motion of viscous liquid in a permeable channel and provided its exact solution. After Berman,[1] numerous scholars have extended his concept for both viscous and non-Newtonian liquids in various directions containing both flat and curved channels. Abbas *et al.*[2] performed an analytical inspection for the magnetohydrodynamic flow Maxwell fluid inside a permeable channel. Ali *et al.*[3] evaluated the effects of applied magnetic field on Oldroyd-B liquid flow inside a channel. Heat transmission analysis in flow of MHD Jeffery liquid through a channel was conveyed by Aleem *et al.*[4] The investigation of the peristaltic flow of Casson liquid via a permeable channel was carried out by Ali *et al.*[5] Hamza *et al.*[6] scrutinized the convective flow of exothermic Arrhenius fluid across a vertical channel. Sajid *et al.*[7] analyzed the influence of Joule heating and magnetic field in the motion of nanoparticles through a curved semi-porous channel. Numerical simulation for the movement of non-Newtonian liquid through a curved channel with Cattaneo–Christov heat flux theory was accomplished by Abbas *et al.*[8] In another article, Abbas *et al.*[9] examined the thermally radiative and convectively heated flow of Carreau liquid via a curved channel. Heat transmission examination for flow of hybrid nanofluid via a curved channel was examined by Abbasi *et al.*[10] Naveed *et al.*[11] investigated the significance of melting heat transmission in the chemically reactive motion of Eyring–Powell liquid inside a curved channel. The study of oscillatory flow is a vital theory in the arena of biological and manufacturing developments such as oil extraction, lung respiratory functions processing, blood flow control during surgical treatment, processing and developing of papers and foods, cosmetic products, chemical and blood allocation modeling in clinical and biochemistry laboratories, *etc*. Misra *et al.*[12] analyzed the heat transport features in a flow of viscoelastic liquid in a oscillatory channel. Ali and Asghar[13] have conducted an analytical inspection for Jef-

[†]Corresponding author. E-mail: imran@ue.edu.pk

© 2026 Chinese Physical Society and IOP Publishing Ltd. All rights, including for text and data mining, AI training, and similar technologies, are reserved.

fery liquid flow over an oscillating channel. Khan *et al.*[14] considered the heat transmission examination in magnetohydrodynamic movement of Maxwell fluid inside an oscillatory channel. Raghunatha and Vinod[15] studied the motion of couple stress fluid inside a porous channel in the presence of the magnetic field. Devi and Srinivas[16] computed heat transferal effects on magnetohydrodynamic oscillatory flow in a porous channel with two immiscible liquids. Naveed *et al.*[17] detected the outcomes of homogeneous heterogeneous chemical reactions in unsteady motion of couple stress liquid through the oscillation of a curved stretched surface. Imran *et al.*[18] assessed the impacts of Soret and Dufour numbers in the oscillatory motion of couple stress liquid due to a curvy wall. In another article, Imran *et al.*[19] inspected the curvilinear oscillatory motion of hybrid nanoliquid over a curved oscillating surface.

To improve the efficiency of modern cooling technology and biomedical or industrial processes that involve heat transfer, it is essential to enhance the thermophysical properties of traditional liquids like ethylene glycol, oil, and water. This can be accomplished by incorporating nano-sized metal particles termed nanoparticles in above-defined liquids. A remarkable number of scholars have paid special attention to detecting the features of such nanoparticles. Abbas *et al.*[20] scrutinized thermal radiation effects in the time-dependent flow of Casson nanoliquid towards a curvy stretched wall. Azam *et al.*[21] detected the three-dimensional (3D) motion of Cross nanoliquid with Cattaneo-Christov heat flux past a moving surface. Inspection of entropy production in a chemically reactive Blasius nanoliquid motion on a curved surface was completed by Naveed *et al.*[22] Sadighi *et al.*[23] conducted heat and mass transport scrutiny for hydromagnetic stretchable nanoliquid motion across flat walls.

The study of heat and mass transport features via revised Fourier and Fick's concepts has engaged noteworthy scholars because of their massive involvement in numerous industrial and manufacturing procedures including food processing, air conditioning, damage of crops, heat exchangers, refrigeration, and equipment power collectors. Imran *et al.*[24] considered the oscillatory flow of non-Newtonian fluid in the presence of thermal and concentration relaxation time parameters. Khan and Mao[25] conducted a comprehensive analysis of nanofluids via Cattaneo–Christov idea across a curved sheet. Abbas *et al.*[26] evaluated the features of the Cattaneo–Christov double diffusive theory in micropolar liquid motion across a curvy Riga sheet. Faisal *et al.*[27] detected the effects of activation energy and entropy production in double-diffusive flow via a stretching cylinder.

In view of the above-mentioned significant applications of oscillatory channel in various technological disciplines, the ultimate objective of this current research is to discuss the features of heat and mass transfer in the bioconvective flow of nanofluid containing motile gyrotactic microorganisms through a semi-porous curved oscillatory channel. The effect of magnetic field is also considered in flow equation. The swimming of the motile organism (bacteria or fungi) generates the density gradient which enhances the heat and mass transfer rate. Heat and mass transfer analysis is carried out by adopting double diffusive theory. For nanofluid, Buongiorno nanofluid model is considered. The effects of pertinent physical variables on curves of velocities, concentration, pressure and temperature are interpreted graphically in detail. Due to curved oscillatory channel the proposed study may be incorporated into massive technological and physical procedures such as lung respiratory function processing, equipment power collectors, oil exploration, heat exchangers, the development and processing of foods and control of blood flow during surgical treatment.

2. Mathematical development

A boundary layer two-dimensional (2D) and time-dependent flow of an incompressible nanoliquid inside a semi-permeable curvy channel of radius A_α is considered (as shown in Fig. 1).

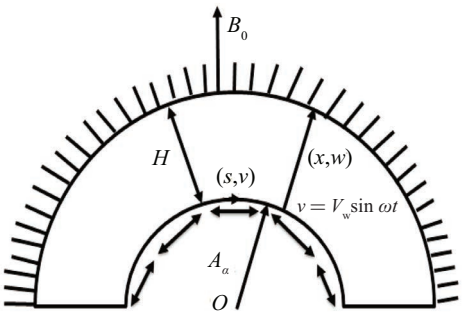


Fig. 1. Flow configuration.

The wall at a distance H of the channel is measured to be permeable and a viscous liquid is injected through it. The lower wall is taken to be oscillatory with periodic velocity $v = V_{\rm w} \sin \omega t$ around the origin, where $V_{\rm w}$ and ω denote the velocity and the frequency of the wall oscillations, respectively. A magnetic field of strength B_0 is imposed in the radial x-direction. The associated boundary layer equations are termed as follows:

$$\frac{\partial v}{\partial s} A_\alpha + \frac{\partial}{\partial x}\{(A_\alpha + x)\, w\} = 0, \tag{1}$$

$$\frac{1}{\rho_\alpha}\frac{\partial p^*}{\partial x} = \frac{v^2}{x + A_\alpha}, \tag{2}$$

$$\frac{\partial v}{\partial t}+\frac{\partial v}{\partial x}w+\frac{vw}{A_\alpha+x}+\left(\frac{A_\alpha v}{A_\alpha+x}\right)\frac{\partial v}{\partial s}=-\frac{A_\alpha}{A_\alpha+x}\frac{1}{\rho_\alpha}\frac{\partial p}{\partial s}-\frac{\sigma_\alpha}{\rho_\alpha}B_0^2 v$$
$$-\frac{1}{\rho_\alpha}(n-n_1)g^*\gamma^*(\rho_{\rm m}-\rho_\alpha)+\nu_\alpha\left(\frac{\partial^2 v}{\partial x^2}-\frac{v}{(A_\alpha+x)^2}+\frac{1}{A_\alpha+x}\frac{\partial v}{\partial x}\right)$$
$$+\frac{1}{\rho_\alpha}\left((1-c_1)\rho_\alpha\beta^*g^*(T-T_1)-(\rho_{\rm p}-\rho_\alpha)g^*(c-c_1)\right), \tag{3}$$

$$\frac{\partial T}{\partial t}+\frac{A_\alpha v}{A_\alpha+x}\frac{\partial T}{\partial s}+\frac{\partial T}{\partial x}w=\kappa\left(\frac{\partial^2 T}{\partial x^2}+\frac{1}{A_\alpha+x}\frac{\partial T}{\partial x}\right)+\frac{\sigma_\alpha}{(\rho c)_p}B_0^2v^2+\varepsilon\left(D_{\rm b}\left(\frac{\partial c}{\partial x}\frac{\partial T}{\partial x}\right)+\frac{D_T}{T_1}\left(\frac{\partial T}{\partial x}\right)^2\right)-\psi_{\rm E}\Omega_{\rm E}, \tag{4}$$

$$\frac{\partial c}{\partial t}+v\left(\frac{A_\alpha}{A_\alpha+x}\right)\frac{\partial c}{\partial s}+\frac{\partial c}{\partial x}w=D_{\rm b}\left(\frac{\partial^2 c}{\partial x^2}+\frac{\partial c}{(A_\alpha+x)\partial x}\right)+\frac{D_T}{T_1}\left(\frac{\partial^2 T}{\partial x^2}+\frac{\partial T}{(A_\alpha+x)\partial x}\right)-\psi_{\rm C}\Omega_{\rm C}, \tag{5}$$

$$\frac{\partial n}{\partial t}+\frac{\partial n}{\partial s}\frac{A_\alpha v}{(A_\alpha+x)}+\frac{\partial n}{\partial x}w=D_{\rm m}\left(\frac{\partial^2 n}{\partial x^2}+\frac{\partial n}{(A_\alpha+x)\partial x}\right)-\frac{b_e W_c}{(c_w-c_1)}\frac{\partial}{\partial x}\left(n\frac{\partial c}{\partial x}\right), \tag{6}$$

where w and v are reflected normal and axial velocity parts, ρ_α and p^* are the density and the pressure of the fluid, which indicate the thermophoretic diffusion, $\rho_{\rm p}$ and $\rho_{\rm m}$ are the density of nanoparticles and the density of microorganisms particles, g^* and γ^* are the gravity and the average volume of microorganisms, β^* is the volume expansion coefficient, $W_{\rm c}$ is the maximum cell swimming velocity, $\Omega_{\rm E}$ and $\Omega_{\rm C}$ are the relaxation of heat and concentration fluxes respectively, κ characterizes the thermal diffusivity, $b_{\rm e}$ is the chemotaxis constant, $c_{\rm p}$ is the specific heat capacity at identical pressure, $D_{\rm b}$ exemplifies the constant factor of Brownian diffusion, $\varepsilon=(c_{\rm p}\rho_{\rm p})/(\rho_{\rm f}c_{\rm f})$ is the relation variable of the heat capability to the material ration of the liquid, v_α is the kinematic viscosity, c and n are the concentrations of nanoparticles and microorganisms, $D_{\rm m}$ is the coefficient of microorganism diffusion, and T is the fluid temperature.

In the above equations, the terms $\psi_{\rm E}$ and $\psi_{\rm c}$ are stated as

$$\psi_{\rm E}=\frac{\partial^2 T}{\partial t^2}+\frac{\partial w}{\partial t}\frac{\partial T}{\partial x}+2w\frac{\partial^2 T}{\partial t\partial x}+\frac{A_\alpha}{x+A_\alpha}\frac{\partial v}{\partial t}\frac{\partial T}{\partial s}+\frac{2A_\alpha v}{x+A_\alpha}\frac{\partial^2 T}{\partial t\partial s}-\frac{vwA_\alpha}{(x+A_\alpha)^2}\frac{\partial T}{\partial s}+w^2\frac{\partial^2 T}{\partial x^2}$$
$$+\frac{v^2A_\alpha^2}{(x+A_\alpha)^2}\frac{\partial^2 T}{\partial s^2}+\left(w\frac{\partial w}{\partial x}+\frac{vA_\alpha}{x+A_\alpha}\frac{\partial w}{\partial s}\right)\frac{\partial T}{\partial x}+\frac{2vwA_\alpha}{x+A_\alpha}\frac{\partial^2 T}{\partial x\partial s}+\left(\frac{A_\alpha w}{x+A_\alpha}\frac{\partial v}{\partial x}+\frac{A_\alpha^2 v}{(x+A_\alpha)^2}\frac{\partial v}{\partial s}\right)\frac{\partial T}{\partial s}, \tag{7}$$

$$\psi_{\rm C}=\frac{\partial^2 c}{\partial t^2}+\frac{\partial w}{\partial t}\frac{\partial c}{\partial x}+2w\frac{\partial^2 c}{\partial t\partial x}+\frac{A_\alpha}{x+A_\alpha}\frac{\partial v}{\partial t}\frac{\partial c}{\partial s}+\frac{2A_\alpha v}{x+A_\alpha}\frac{\partial^2 c}{\partial t\partial s}-\frac{vwA_\alpha}{(x+A_\alpha)^2}\frac{\partial c}{\partial s}+w^2\frac{\partial^2 c}{\partial x^2}$$
$$+\frac{v^2A_\alpha^2}{(x+A_\alpha)^2}\frac{\partial^2 c}{\partial s^2}+\left(w\frac{\partial w}{\partial x}+\frac{vA_\alpha}{x+A_\alpha}\frac{\partial w}{\partial s}\right)\frac{\partial c}{\partial x}+\frac{2vwA_\alpha}{x+A_\alpha}\frac{\partial^2 c}{\partial x\partial s}+\left(\frac{A_\alpha w}{x+A_\alpha}\frac{\partial v}{\partial x}+\frac{A_\alpha^2 v}{(x+A_\alpha)^2}\frac{\partial v}{\partial s}\right)\frac{\partial c}{\partial s}, \tag{8}$$

The correlated boundary conditions are

$$\begin{aligned}&T=T_{\rm w},\quad v=(\sin\omega t)V_{\rm w},\quad c=c_{\rm w},\quad n=n_{\rm w},\quad 0=w,\quad \text{at } x=0,\\&0=v,\quad T\to T_1,\quad w=\frac{-V_{\rm w}}{(A_\alpha+x)}\frac{A_\alpha}{},\quad c\to c_1,\quad n=n_1,\quad \text{as } x=H,\end{aligned} \tag{9}$$

where, $V_{\rm w}<0$ signifies injection and $V_{\rm w}>0$ designates the suction velocity respectively.

We will now commence the following non-dimensional constants as

$$\begin{aligned}&\frac{x}{H}=y,\quad F_y(y,\tau)\frac{V_{\rm w}s}{H}=v,\quad t\omega=\tau,\quad \frac{-A_\alpha V_{\rm w}}{A_\alpha+x}F(y,\tau)=w,\quad \frac{\rho_\alpha V_{\rm w}^2 s^2}{H^2}P^*(y,\tau)=p,\\&T-T_1=(T_{\rm w}-T_1)\theta(y,\tau),\quad n-n_1=(n_{\rm w}-n_1)\chi(y,\tau),\quad c-c_1=(c_{\rm w}-c_1)\varphi(y,\tau).\end{aligned} \tag{10}$$

Through the devotion of Eq. (10), equation (1) is validated, and lasting equations (2)–(6) yields

$$P_y^*=\frac{1}{(C_0+y)}F_y^2, \tag{11}$$

$$P^*(y,\tau)=\frac{C_0+y}{2C_0Re}\begin{pmatrix}F_{yyy}+\dfrac{F_{yy}}{(y+C_0)}-\dfrac{F_y}{(y+C_0)^2}-M^2F_y-SF_{y\tau}\\-F_y^2\dfrac{\beta}{(y+C_0)}+\dfrac{\beta}{(y+C_0)}FF_{yy}+FF_y\dfrac{\beta}{(y+C_0)^2}\\+\lambda(\theta-Nr\varphi-R_{\rm b}\chi)\end{pmatrix}, \tag{12}$$

$$\frac{1}{Pr}\left(\theta_{yy}+\frac{\theta_y}{(y+C_0)}\right)+Re\left(\frac{C_0F\theta_y}{(y+C_0)}+M^2EcF_y^2-S\theta_\tau\right)+\left(N_t\theta_y^2+N_b\theta_y\varphi_y\right)$$
$$-\alpha_1\left(\begin{array}{l}S^2\theta_{\tau\tau}-\dfrac{SC_0}{(C_0+y)}F_\tau\theta_y-\dfrac{2SC_0}{(C_0+y)}F\theta_{y\tau}+\dfrac{C_0^2}{(C_0+y)^2}F^2\theta_{yy}\\+\dfrac{C_0^2}{(y+C_0)^2}F_yF\theta_y-\dfrac{C_0^2}{(y+C_0)^3}F^2\theta_y\end{array}\right)=0, \tag{13}$$

$$\frac{1}{Le}\left(\varphi_{yy}+\frac{\varphi_y}{(y+C_0)}\right)+Re\left(\frac{C_0}{(y+C_0)}F\varphi_y-\varphi_\tau S\right)+\frac{N_t}{L_eN_b}\left(\theta_{yy}+\frac{\theta_y}{(C_0+y)}\right)$$
$$-\alpha_2\left(\begin{array}{l}\varphi_{\tau\tau}S^2-\dfrac{SC_0}{(C_0+y)}\varphi_yF_\tau-\dfrac{2SC_0}{(C_0+y)}F\varphi_{y\tau}+\dfrac{C_0^2}{(C_0+y)^2}F^2\varphi_{yy}\\+\dfrac{C_0^2}{(y+C_0)^2}F_yF\varphi_y-\dfrac{C_1^2}{(y+C_0)^3}F^2\varphi_y\end{array}\right)=0, \tag{14}$$

$$\frac{1}{L_b}\left(\chi_{yy}+\frac{\chi_y}{(y+C_0)}\right)-ReS\chi_\tau-\frac{P_e\chi_{yy}\delta}{L_b}-\frac{P_e\varphi_{yy}\chi}{L_b}-\frac{P_e\varphi_y\chi_y}{L_b}+Re\frac{C_0}{(y+C_0)}F\chi_y=0, \tag{15}$$

where, $C_0\,(=A_\alpha/H)$ implies the term of the radius of curvature, $N_t\ \left(=\varepsilon D_T\left(T_w-T_1\right)/\nu_\alpha T_1\right)$ is the thermophoresis constant, $Le\ \left(=\nu_\alpha/D_b\right)$ is the Lewis number, $Pr\ \left(=\nu_\alpha/\kappa\right)$ is the Prandtl number, $N_r\ \left(=\left(\rho_p-\rho_\alpha\right)\left(c_w-c_1\right)/\beta^*\rho_\alpha\left(1-c_1\right)\left(T_w-T_1\right)\right)$ is the buoyancy ratio parameter, $S\ \left(=H\omega/V_w\right)$ is the relation of the wall oscillation frequency to the wall velocity, $Re\ \left(=HV_w/\nu_\alpha\right)$ is the Reynolds number, $Pe\ \left(=b_eW_c/D_m\right)$ is the Peclet number, $M^2\ \left(=\sigma_\alpha B_0^2H/\rho_\alpha V_w\right)$ is the magnetic parameter, $\lambda\ \left(=H^2\beta^*g^*\left(1-c_1\right)\left(T_w-T_1\right)/V_w^2s\right)$ is the mixed convection parameter, $Ec\ \left(=V_w^2s^2/c_p\left(T_w-T_1\right)H^2\right)$ is the Eckert number, $\alpha_1\ \left(=\Omega_EV^2/\nu_\alpha\right)$ and $\alpha_2\ \left(=\Omega_cV^2/\nu_\alpha\right)$ are the thermal and concentration relaxation parameters, $R_b\ \left(=\gamma^*\left(\rho_m-\rho_\alpha\right)\left(n_w-n_1\right)/\beta^*\rho_\alpha\left(1-c_1\right)\left(T_w-T_1\right)\right)$ is the bioconvection Rayleigh number, $L_b\ \left(=\nu_\alpha/D_m\right)$ is the bioconvection Lewis number, $\delta\ \left(=n_1/\left(n_w-n_1\right)\right)$ is the microorganism concentration difference parameter, and $N_b\ \left(=\varepsilon D_b\left(c_w-c_1\right)/\nu_\alpha\right)$ represents the parameter of Brownian motion.

After confiscating the pressure term from Eqs. (11) and (12), the velocity equation can be determined in the following expression:

$$F_{yyyy}+\frac{2F_{yyy}}{(C_0+y)}-\frac{F_{yy}}{(C_0+y)^2}+\frac{F_y}{(C_0+y)^3}-\left(F_{yy\tau}+\frac{F_{y\tau}}{C_0+y}\right)SRe-\frac{ReC_0F_yF_{yy}}{(C_0+y)}$$
$$+\frac{ReC_0F_{yyy}F}{(C_0+y)}-\frac{C_0ReF_y^2}{(C_0+y)^2}+\frac{C_0ReF_{yy}F}{(C_0+y)^2}+\lambda Re\left(\theta_y+\frac{\theta}{C_0+y}\right)-M^2ReF_{yy}$$
$$-\frac{M^2ReF_y}{C_0+y}-\frac{C_0ReF_yF}{(C_0+y)^3}-\lambda ReNr\left(\varphi_y+\frac{\varphi}{C_0+y}\right)-\lambda ReR_b\left(\chi_y+\frac{\chi}{C_0+y}\right)=0, \tag{16}$$

with the following boundary conditions:

$$\begin{aligned}&\theta(0,\tau)=1,\ \ F_y(0,\tau)=\sin\tau,\ \ \chi(0,\tau)=1,\ \ \varphi(0,\tau)=1,\\&F(0,\tau)=0,\ \ F_y(1,\tau)=\theta(1,\tau)=\chi(1,\tau)=\varphi(1,\tau)=0,\\&F(1,\tau)=1.\end{aligned} \tag{17}$$

The physical quantities along the curved wall are specified by the following expressions:

$$\begin{aligned}&C_F=\frac{\tau_{xs}}{\rho_\alpha V_w^2},\ \ Nu_s=\frac{sq_w}{(T_w-T_1)k_\alpha^*},\\&Sh_s=\frac{sj_w}{(c_w-c_1)D_b},\ \ Nn_s=\frac{sq_n}{(n_w-n_1)D_m},\end{aligned} \tag{18}$$

where τ_{xs}, q_w, q_n, and j_w are depicted by

$$\tau_{xs}=\mu\left(\frac{\partial v}{\partial x}-\frac{v}{A_\alpha+x}\right)\Big|_{x=0},\ \ q_w=-\left(k_\alpha^*\frac{\partial T}{\partial x}\right)\Big|_{x=0},$$

$$q_n=-\left(D_m\frac{\partial n}{\partial x}\right)\Big|_{x=0},\ \ j_w=-\left(D_b\frac{\partial C}{\partial x}\right)\Big|_{x=0}. \tag{19}$$

Making use of Eq. (10) in Eqs. (18) and (19), we attain

$$Re_s^{1/2}C_F=\frac{1}{C_0}\left[C_0F_{yy}(0,\ \tau)-F_y(0,\tau)\right], \tag{20}$$
$$Re_s^{-1/2}Nu_s=-\theta_y(0,\tau), \tag{21}$$
$$Re_s^{-1/2}Sh_s=-\varphi_y(0,\tau), \tag{22}$$
$$Re_s^{-1/2}Nn_s=-\chi_y(0,\tau), \tag{23}$$

where $Re_s^{1/2}=V_w\,s/\nu_\alpha$ represents the Reynolds number.

3. Solution methodology

The key motivation of this segment of the novel is to concisely explicate the approach that we incorporate to compute the resolution of leading nonlinear partial differential equa-

tions (13)–(16) with ultimate boundary conditions (17). For this delineation, we induct the following expressions:

$$\begin{aligned}
&F_0(y,\tau) = (\sin\tau - 2)y^3 - (2\sin\tau - 3)y^2 + (\sin\tau)y,\\
&\varphi_0(y,\tau) = (1-y),\ \ \chi_0(y,\tau) = (1-y),\\
&\theta_0(y,\tau) = (1-y), \qquad (24)\\
&\boldsymbol{N}_{\mathrm{F}}(F) = F_{yyyy},\ \ \boldsymbol{N}_{\theta}(\theta) = \theta_{yy},\ \ \boldsymbol{N}_{\chi}(\chi) = \chi_{yy},\\
&\boldsymbol{N}_{\varphi}(\varphi) = \varphi_{yy} \qquad (25)
\end{aligned}$$

with

$$\begin{aligned}
&\boldsymbol{N}_{\mathrm{F}}\left[A_4y^3 + A_3y^2 + A_2y + A_1\right] = 0,\\
&\boldsymbol{N}_{\theta}\left[A_6y + A_5\right] = 0,\\
&\boldsymbol{N}_{\varphi}\left[A_8y + A_7\right] = 0,\\
&\boldsymbol{N}_{\chi}\left[A_{10}y + A_9\right] = 0. \qquad (26)
\end{aligned}$$

The general solution is given as

$$F_{\mathrm{r}}^{*}(y,\tau) = F_{\mathrm{r}}(y,\ \tau) + A_1 + A_2y + A_3y^2 + A_4y^3, \qquad (27)$$

$$\theta_{\mathrm{r}}^{*}(y,\tau) = \theta_{\mathrm{r}}(y,\tau) + A_5 + A_6y, \qquad (28)$$

$$\varphi_{\mathrm{r}}^{*}(y,\tau) = \phi_{\mathrm{r}}(y,\tau) + A_7 + A_8y, \qquad (29)$$

$$\chi_{\mathrm{r}}^{*}(y,\tau) = \chi_{\mathrm{r}}(y,\tau) + A_9 + A_{10}y, \qquad (30)$$

where $F_{\mathrm{r}}(y,\tau)$, $\theta_{\mathrm{r}}(y,\tau)$, $\chi_{\mathrm{r}}(y,\tau)$, and $\varphi_{\mathrm{r}}(y,\tau)$ suggest a particular solution. With the help of ending boundary conditions, the constants A_i $(i = 1,2,3,4,5,6,7,8,9,10)$ are computed as follows:

$$\begin{aligned}
&A_1 = -F_{\mathrm{r}}(0,\tau),\ A_2 = -\frac{\partial F_{\mathrm{r}}(0,\tau)}{\partial y},\\
&A_3 = \frac{2\partial F_{\mathrm{r}}(0,\tau)}{\partial y} + \frac{\partial F_{\mathrm{r}}(1,\tau)}{\partial y} + 3F_{\mathrm{r}}(0,\tau) - 3F_{\mathrm{r}}(1,\tau),\\
&A_4 = -\frac{\partial F_{\mathrm{r}}(1,\tau)}{\partial y} + 2F_{\mathrm{r}}(1,\tau) - \frac{\partial F_{\mathrm{r}}(0,\tau)}{\partial y} - 2F_{\mathrm{r}}(0,\tau),\\
&A_5 = -\theta_{\mathrm{r}}(0,\tau),\ A_6 = \theta_{\mathrm{r}}(0,\tau) - \theta_{\mathrm{r}}(1,\tau),\\
&A_7 = -\varphi_{\mathrm{r}}(0,\tau),\ A_8 = \varphi_{\mathrm{r}}(0,\tau) - \varphi_{\mathrm{r}}(1,\tau),\\
&A_9 = -\chi_{\mathrm{r}}(0,\tau),\ A_{10} = \chi_{\mathrm{r}}(0,\tau) - \varphi_{\mathrm{r}}(1,\tau). \qquad (31)
\end{aligned}$$

3.1. Results and discussion

This part of the novel briefly enlighten the upshots of numerous involved parameters comprising the radius of curvature variable C_0, thermophoresis parameter N_{t}, Reynolds number Re, proportion of oscillatory wall frequency to the velocity of the wall constant S, dimensionless Lewis number Le, buoyancy ratio parameter N_{r}, magnetic parameter M, Peclet number Pe, Brownian motion parameter N_{b}, bioconvection Lewis number L_{b}, Prandtl number Pr, mixed convective parameter λ, thermal relaxation parameter α_1, Eckert number Ec, bioconvection Rayleigh number R_{b}, concentration relaxation parameter α_2, microorganism concentration difference variable δ on pressure field, liquid velocity field, concentration distribution, microorganism distribution profile, temperature distribution, skin friction coefficient, rate of communication of heat and mass via tables and graphs.

Table 1 illuminates that the arithmetic magnitude of $C_{\mathrm{F}}Re_{\mathrm{s}}^{1/2}$ shrinks for improving values of R_{b}, N_{r}, and M, and it inclines up with Re, C_0, and λ at $\tau = 0.5\pi$. Table 2 highlights a growing trend in the magnitude of the heat transfer rate under the influence of Re, and C_0, and for upward values of α_1, N_{t}, Pr, Ec, and N_{b}, the magnitude of the rate of heat transmission coefficient falls downward.

Table 1. Numerical assessment of $C_{\mathrm{F}}Re_{\mathrm{s}}^{1/2}$ for some values of Re, R_{b}, C_0, N_{r}, λ, and M by using $Pr = Le = Ec = Pe = L_{\mathrm{b}} = \delta = S = 0.5, \alpha_1 = \alpha_2 = N_{\mathrm{t}} = N_{\mathrm{b}} = 0.1$ at $\tau = 0.5\pi$.

Re	R_{b}	C_0	N_{r}	λ	M	$C_{\mathrm{F}}Re_{\mathrm{s}}^{1/2}$
0.5	0.3	1.0	0.1	0.5	0.1	1.04370
2.0						1.06646
3.5						1.08923
0.5	0.5					1.04355
	1.5					1.04280
	2.5					1.04205
	0.3	1.5				1.41827
		2.0				1.63854
		2.5				1.80096
		1.0	0.5			1.04340
			1.5			1.04265
			2.5			1.04190
			0.1	0.2		1.04343
				0.6		1.04379
				1.0		1.04415
				0.5	0.5	1.04364
					2.0	1.04268
					3.5	1.04060

Table 2. Numerical assessment of $Nu_{\mathrm{s}}Re_{\mathrm{s}}^{-1/2}$ for some values of α_1, Pr, Re, N_{t}, C_0, Ec, and N_{b} by using $S = M = \lambda = Le = Pe = L_{\mathrm{b}} = \delta = 0.5, \alpha_2 = R_{\mathrm{b}} = N_{\mathrm{r}} = 0.1$ at $\tau = 0.5\pi$.

α_1	P_{r}	Re	N_{t}	C_0	Ec	N_{b}	$Nu_{\mathrm{s}}Re_{\mathrm{s}}^{-1/2}$
0.1	1.0	0.5	0.1	1.0	0.5	0.2	1.01245
0.3							1.01165
0.5							1.01086
0.1	1.5						1.00964
	2.0						1.00683
	2.5						1.00402
	1.0	1.0					1.01490
		2.5					1.02228
		4.0					1.02967
		0.5	0.2				1.00989
			0.5				1.00221
			0.8				0.99454
			0.1	0.5			1.00576
				1.5			1.01938
				2.5			1.02581
				1.0	0.1		1.01409
					0.4		1.01286
					0.7		1.01163
					0.5	0.1	1.01501
						0.3	1.00989
						0.5	1.00476

Figures 2(a) and 2(b) are constructed to elaborate the three-dimensional (3D) reflection of the physical de-manner

of the axial velocity component $v(x,t)$ over the lower oscillatory and upper porous wall of the channel by assuming $x \to 0$ and $x = 1$.

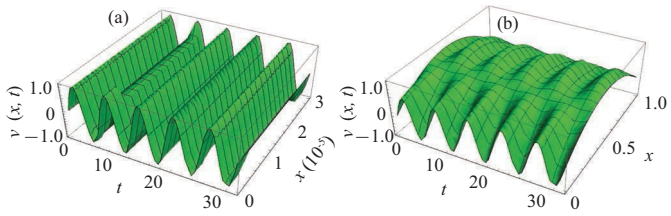


Fig. 2. The 3D view of$v(x,t)$(a) for lower curvy oscillatory wall (b) for upper permeable wall. For lower wall $x = 3 \times 10^{-5}$ and for upper wall $x = 1$.

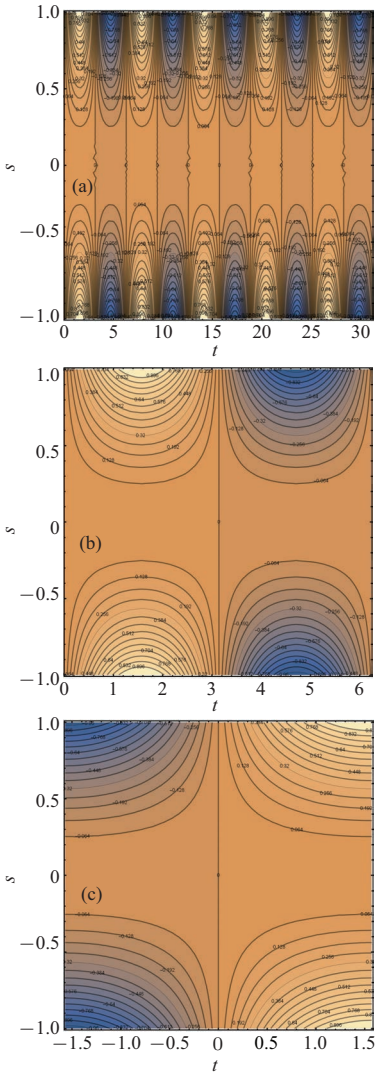


Fig. 3. Distinctions in streamlines of $v(x,t)$ by taking $x \to 0$, *i.e.*, $x = 3 \times 10^{-5}$ with $C_0 = R_b = Pr = Le = Pe = 1.0$, $M = N_b = \lambda = Ec = \delta = L_b = 0.5$, $Re = 3.0$, $N_t = \alpha_1 = \alpha_2 = 0.1$, and $S = 1.0$. (a) $t \in (0, 10\pi)$, (b) $t \in (0, 2\pi)$, and (c) $t \in (-0.5\pi, 0.5\pi)$.

Figures 3(a)–3(c) and 4(a)–4(c) characterize that the streamlines of velocity components show a symmetrical manner and deviate from the origin for a time interval $t \in [-0.5\pi, 0.5\pi]$, and remarked oscillatory response for $t \in [0, 10\pi]$ and $t \in [0, 2\pi]$ respectively.

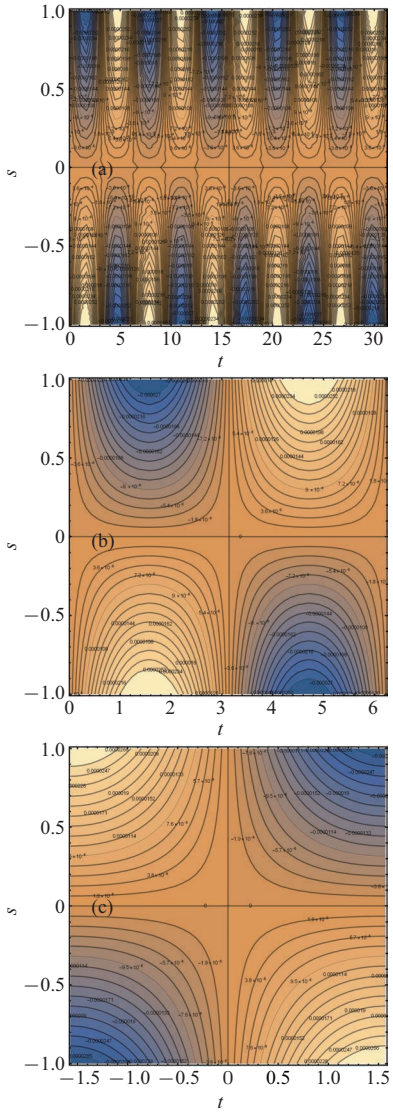


Fig. 4. Variations in stream lines of $v(x,t)$ by taking $x \to 0$, *i.e.*, $x = 3 \times 10^{-5}$ with $C_0 = R_b = Pr = Le = Pe = 1.0$, $M = N_b = \lambda = Ec = \delta = L_b = 0.5$, $Re = 3.0$, $N_t = \alpha_1 = \alpha_2 = 0.1$, and $S = 1.0$. (a) $t \in (0, 10\pi)$, (b) $t \in (0, 2\pi)$, and (c) $t \in (-0.5\pi, 0.5\pi)$.

Figures 5(a)–5(d) give the results of disparate flow variables like C_0, λ, Re, and S on $F'(y,\tau)$ for $y = 0.1$ from the wall of the channel. It is perceived from this figure that $F'(y,\tau)$ amplitude depicts an uphill manner with upward values of S and λ. Whereas, $F'(y,\tau)$ amplitude is diminished with Re and C_0.

The significances of R_b, C_0, N_r, M, Re, S, and λ on $F'(y,\tau)$ at $\tau = 0.5\pi$ are expounded via Figs. 6(a)–6(d). This graph viewed that with elevating values of C_0, λ, and Re, the liquid profile $F'(y,\tau)$ initially grows, but after $y = 0.5$ it illustrates reducing behavior. However, for varying values of M, N_r, R_b and S, the $F'(y,\tau)$ profile shows a contrary response.

Figures 7(a)–7(d) clarify that the amplitude of $P^*(y,\tau)$ enlarges with upward values of Re and declines for N_r, M, and R_b in time intervals $\tau \in (0, 10\pi)$. One can detect from Figs. 8(a)–8(d) that $P^*(y,\tau)$ is a reducing function of C_0, λ, M, and Re and $P^*(y,\tau)$ improves with improving values of R_b and at $\tau = 0.5\pi$.

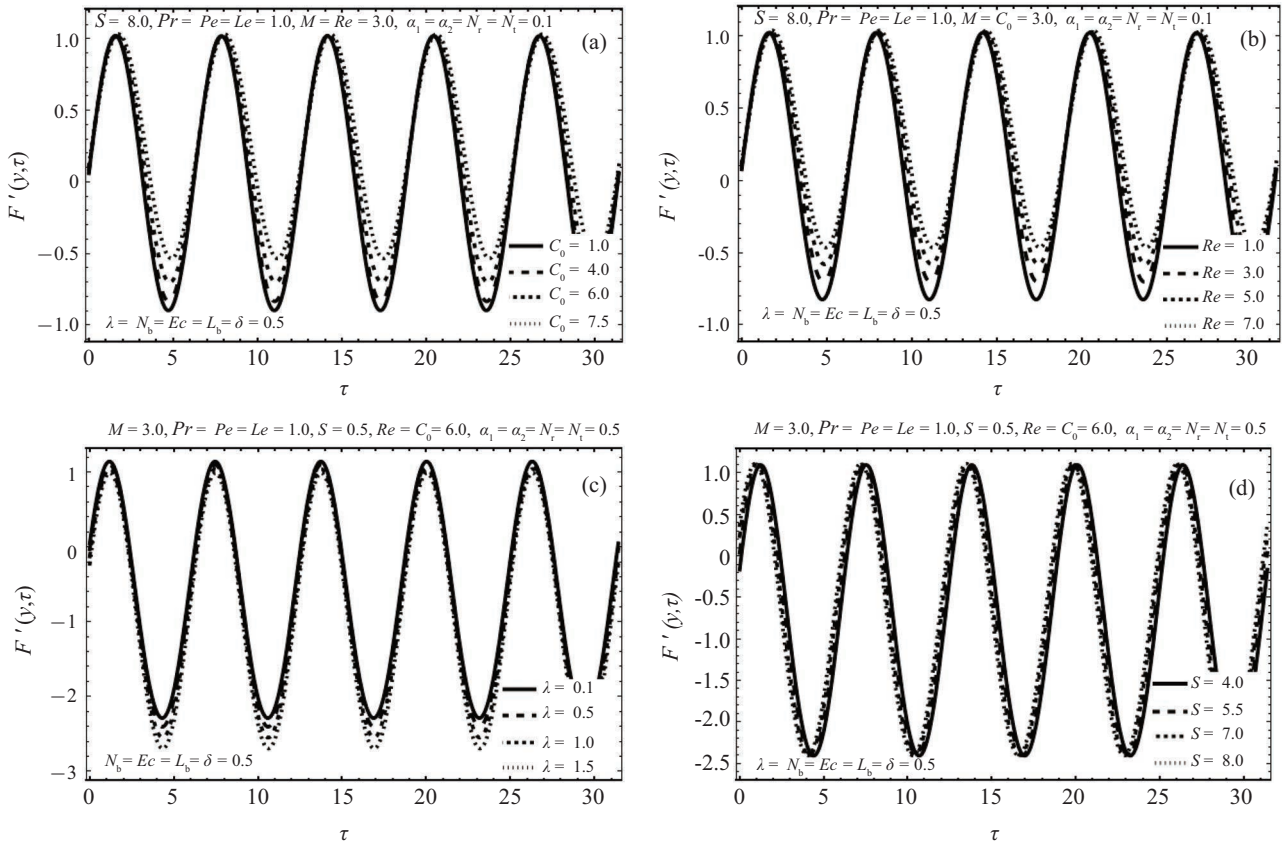


Fig. 5. The variation in velocity field $F'(y,\tau)$ at $\tau = (0, 10\pi)$ for (a) effect of C_0, (b) effect of Re, and (c) effect of λ, and (d) effect of S.

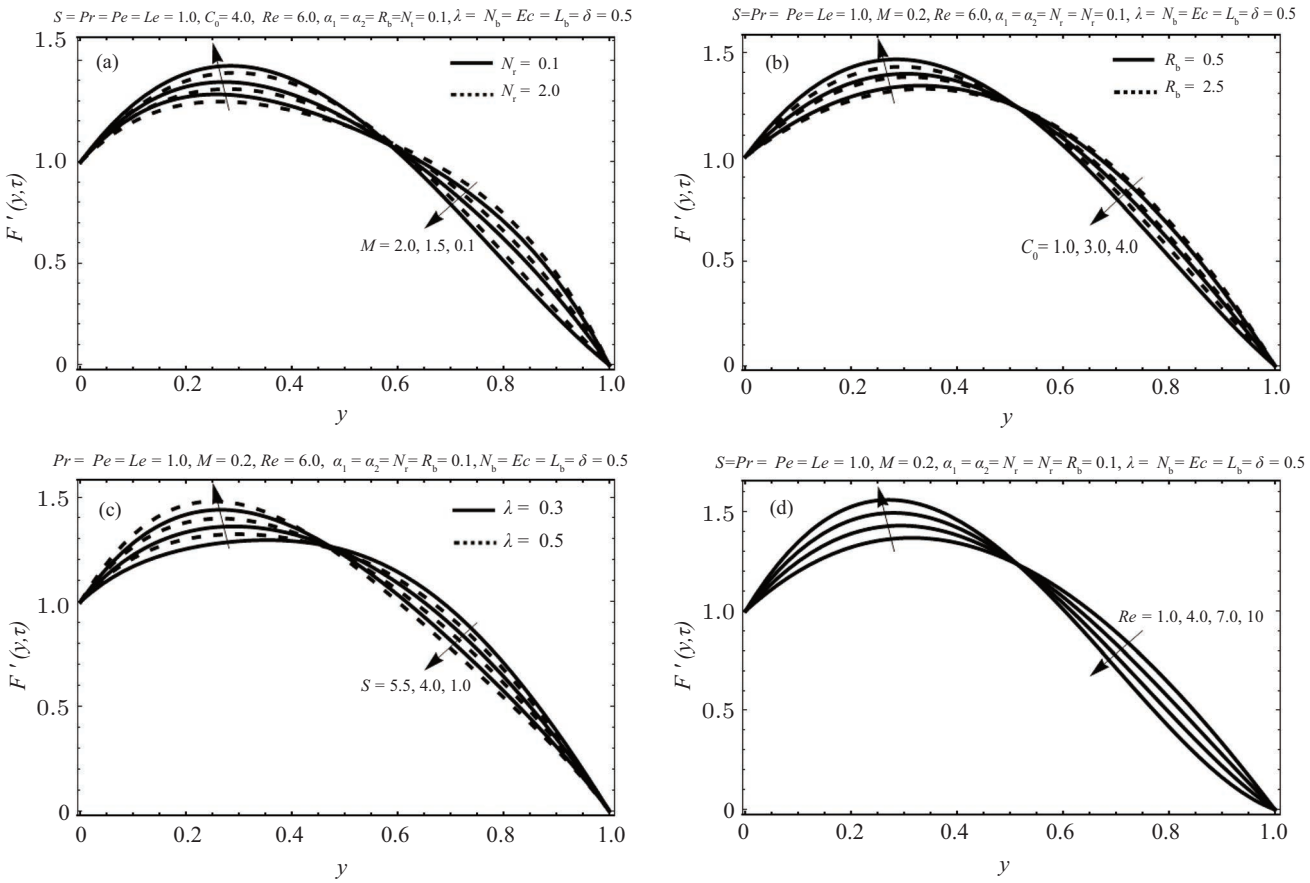


Fig. 6. The variation in velocity field $F'(y,\tau)$ at $\tau = 0.5\pi$ for (a) effects of M and N_r, (b) effects of C_0 and R_b, (c) effects of S and λ, and (d) effects of Re.

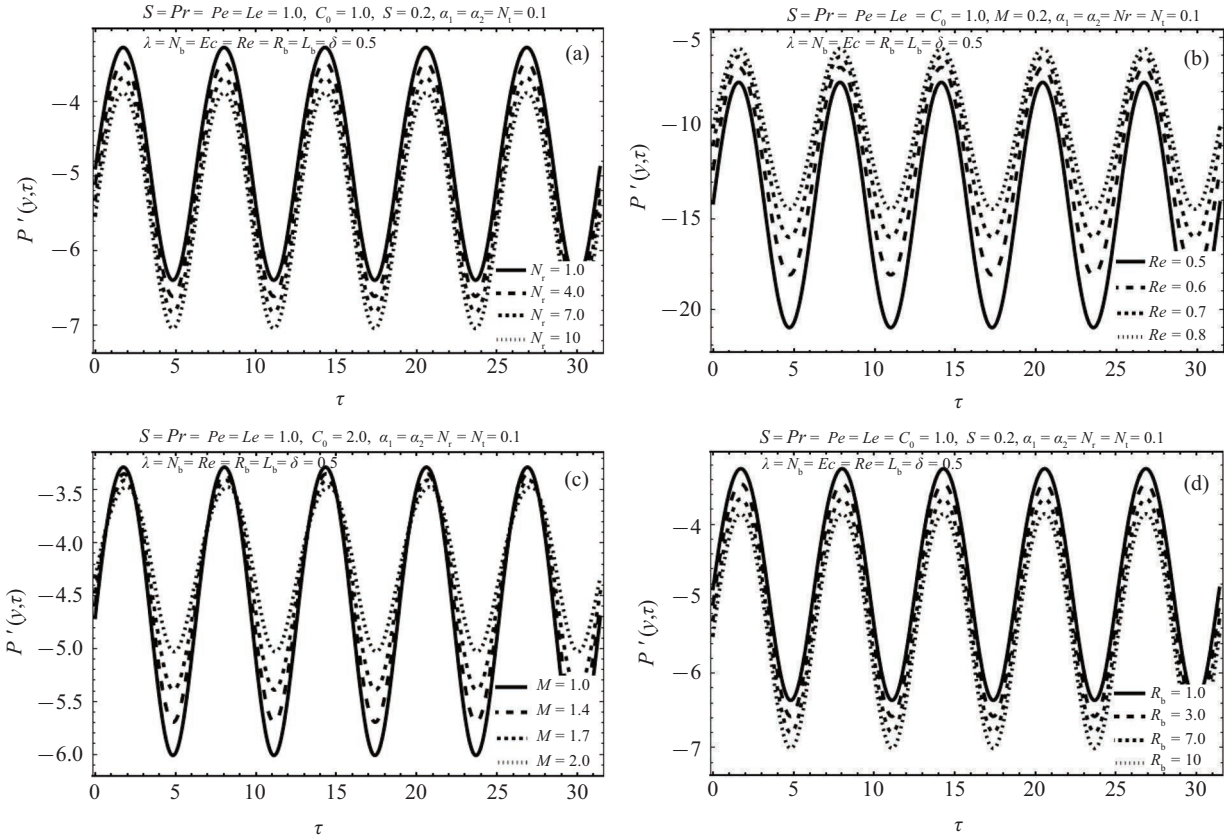


Fig. 7. The variation in pressure profile $P(y,\tau)$ at $\tau \in (0, 10\pi)$ for (a) effects of Nr, (b) effects of Re, (c) effects of M, and (d) effects of $R_{\rm b}$.

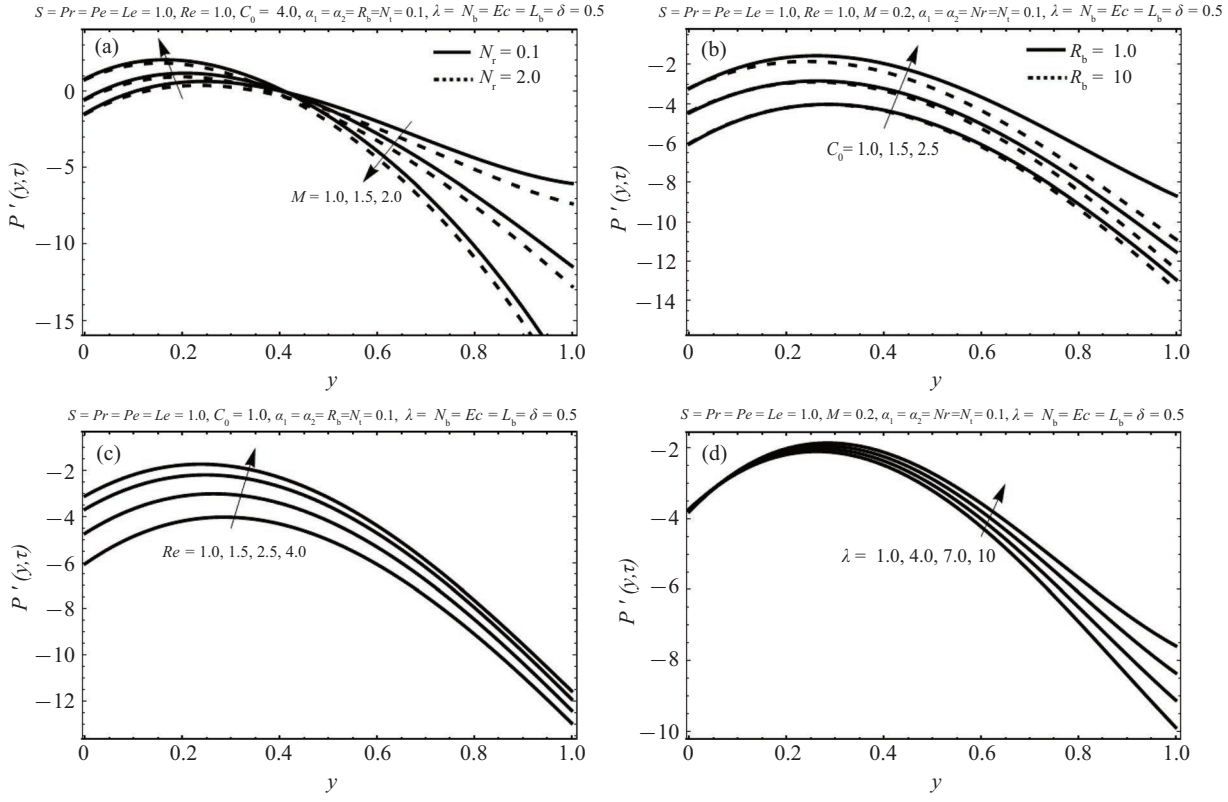


Fig. 8. The variation in pressure profile $P(y,\tau)$ at $\tau = 0.5\pi$ for (a) effects of M and $N_{\rm r}$, (b) effects of C_0 and $R_{\rm b}$, (c) effects of Re, and (d) effects of λ.

Figures 9(a)–9(d) identify the response of the liquid temperature profile $\theta(y,\tau)$ due to the varying values of dissimilar variables in the time interval $\tau = 0.5\pi$. It is perceived from this figure that the temperature of the liquid shows a positive trend with growing values of $N_{\rm t}$, Ec, α_1, $N_{\rm b}$, and M, and it declines with altering values of the Reynolds number Re, the Prandtl number Pr, and the parameter C_0.

The change in concentration profile under the influence of various involved parameters likely N_t, Pr, C_0, α_2, Le, Re, S, and N_b is noticed in Figs. 10(a)–10(d). This figure witnesses that with upward values of N_t, Pr, Le, Re, S, C_0, and N_b, the profile $\varphi(y,\tau)$ presents falling fashion. However, it inclines gradually for α_2.

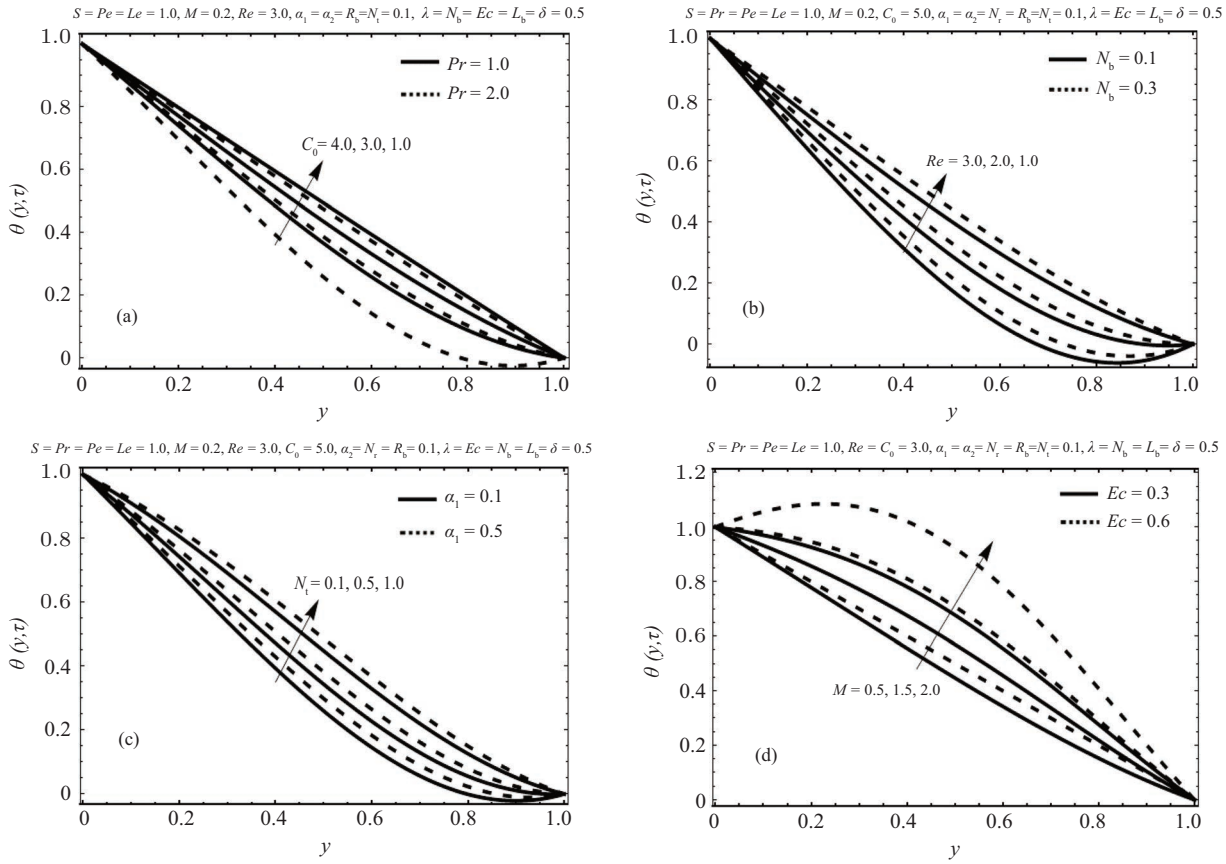


Fig. 9. The variation in temperature profile $\theta(y,\tau)$ for $\tau = 0.5\pi$. (a) Effects of C_0 and Pr, (b) effects of Re and N_b, (c) effects of N_t and α_1, and (d) effects of M and Ec.

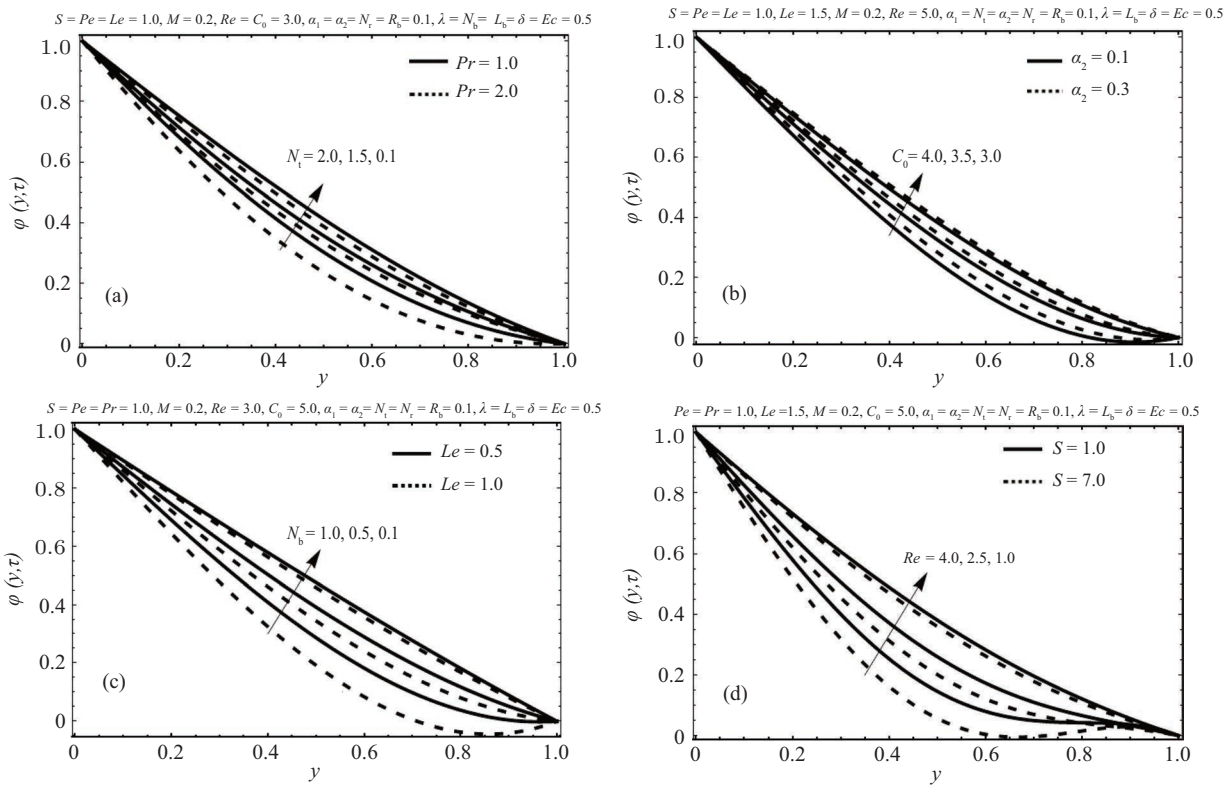


Fig. 10. The variation in concentration profile $\varphi(y,\tau)$ for $\tau = 0.5\pi$. (a) Effects of N_t and Pr, (b) effects of C_0 and α_2, (c) effects of N_b and L_e, and (d) effects of Re and S.

Figures 11(a)–11(d) are portrayed to explain the outcomes of dissimilar variables such as Pe, C_0, L_b, δ, Re, and S on the microorganism profile $\chi(y,\tau)$. This figure depicts that the microorganism profile is declined with all the above-mentioned variables.

The consequences of the Lewis number Le versus N_b and the Prandtl number Pr versus N_t on the local Sherwood number are scrutinized via Figs. 12(a)–12(d). It can be observed from this figure that for higher values of the Prandtl number, the magnitude of the local Sherwood number shows a contrary manner, and it demonstrates increasing fashion for the other mentioned variables.

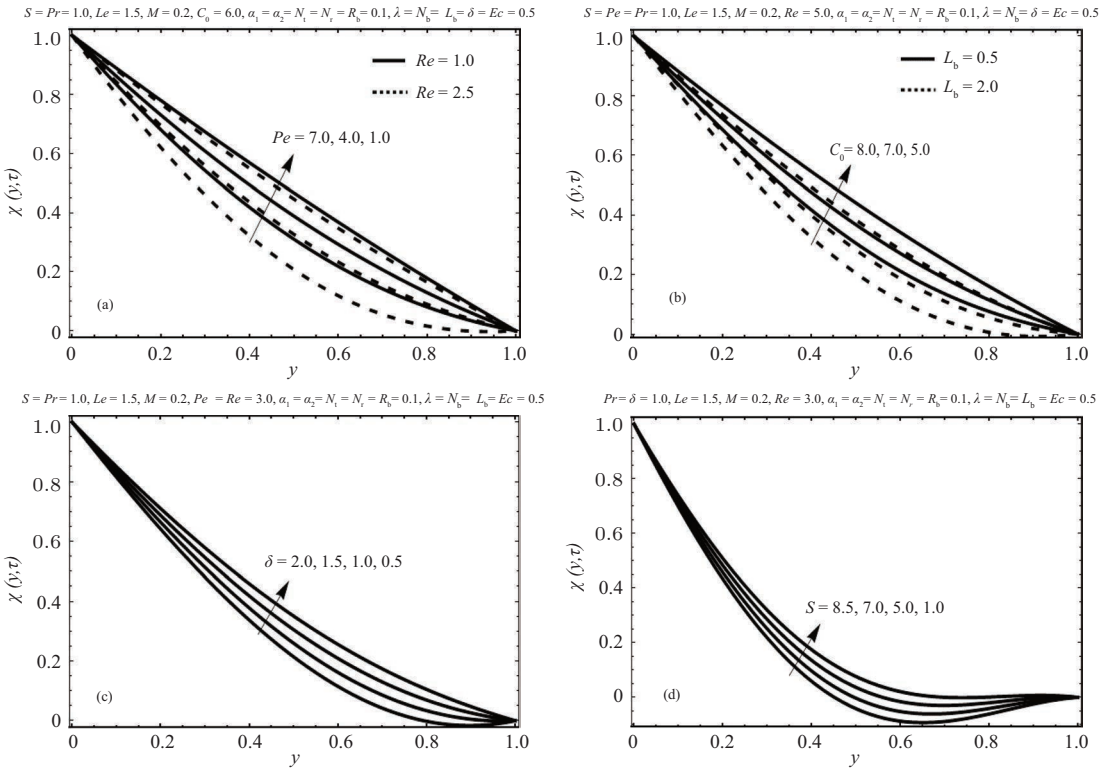


Fig. 11. The variation in microorganism profile $\chi(y,\tau)$ for $\tau = 0.5\pi$. (a) Effects of Pe and Re, (b) effects of C_0 and L_b, (c) effects of δ, and (d) effects of S.

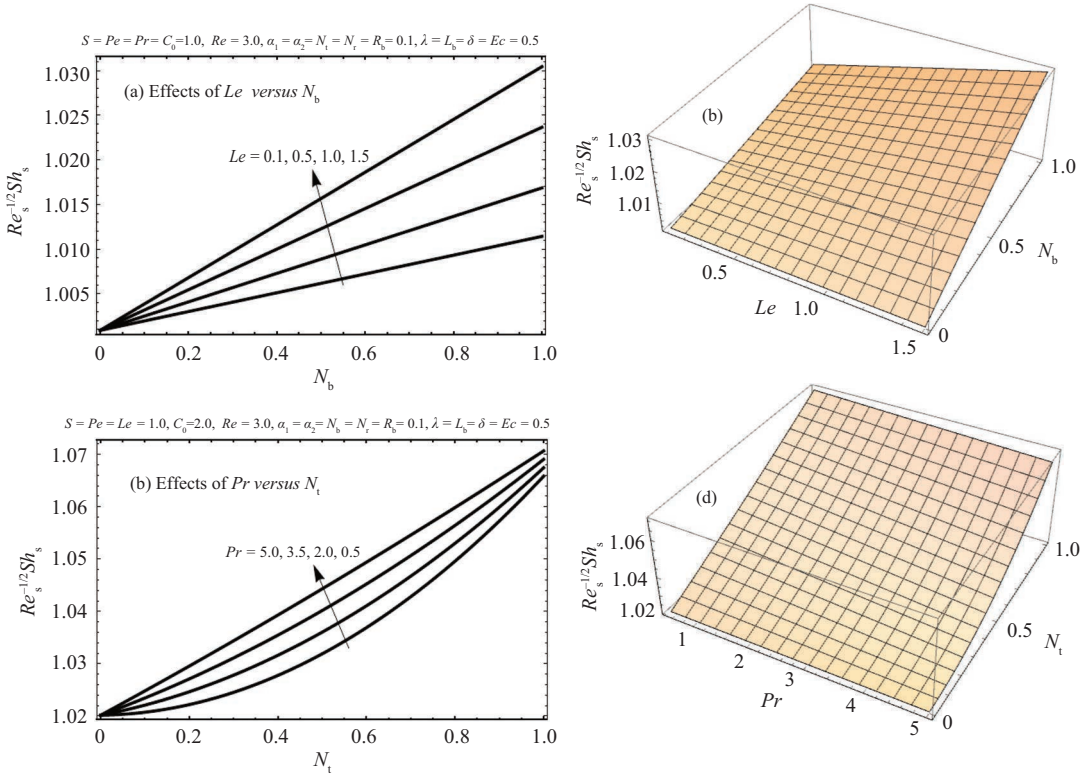


Fig. 12. The variation in Sherwood number $Re_s^{-1/2}Sh_s$ for $\tau = 0.5\pi$.

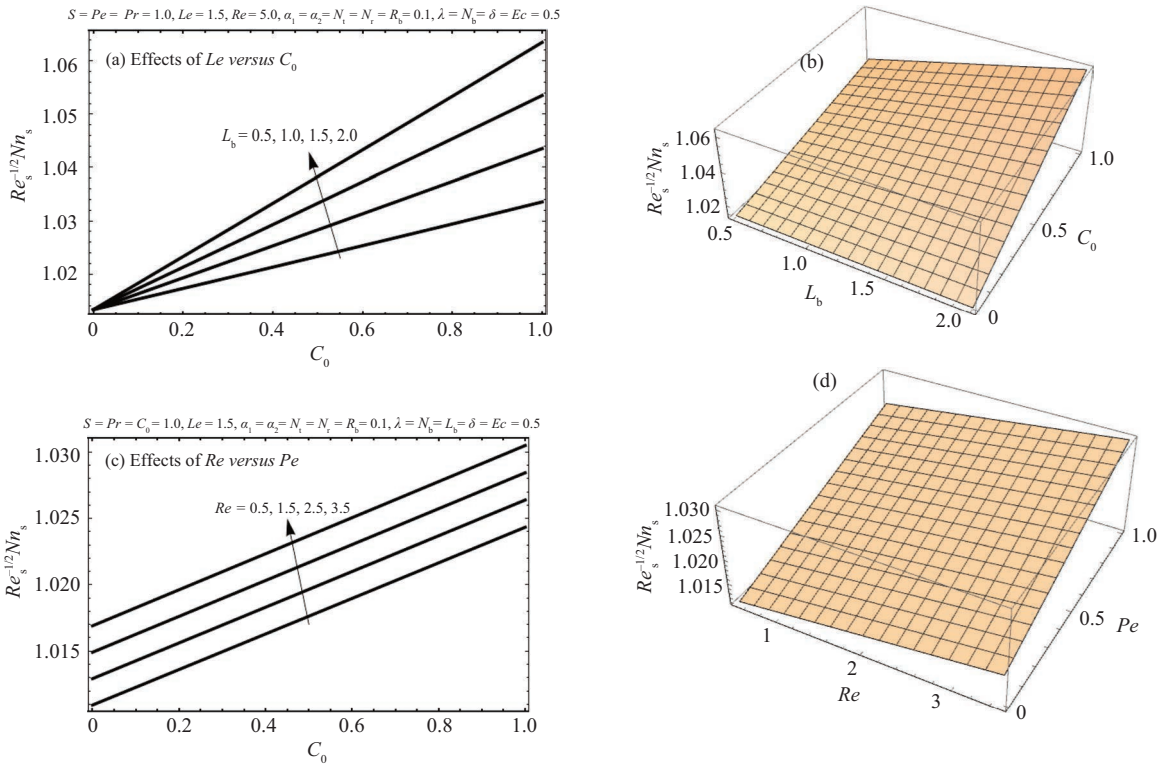


Fig. 13. The variation in Motile number $Re_s^{-1/2}Nn_s$ for $\tau = 0.5\pi$.

Figures 13(a)–13(d) present the alteration in the magnitude of the local Motile number under the consequences of divergent parameters such as L_b versus C_0 and the Reynolds number Re versus Pe. For increasing values of all defined parameters, the magnitude of the local Motile number elucidates a positive trend.

4. Conclusions

In this research communication, we have scrutinized the features of motile gyrotactic microorganisms and relaxation of heat and concentration fluxes on nanoliquid motion by incorporating Buongiorno's concept in a semi-permeable curved oscillatory channel. The following specific conclusions are predicted.

(i) The velocity amplitude portrays falling demeanor with rising values of λ, C_0, and Re. Whereas, it develops with S.

(ii) The liquid velocity profile states enhancing behavior for growing Re and C_0 at $\tau = \pi/2$. However, it displays decreasing reaction with R_b, M, Nr, and S.

(iii) For uplifting values of Re the pressure field amplitude amplifies. While, it diminishes with Nr, M, and R_b.

(iv) At $\tau = 0.5\pi$, the pressure profile is reduced with altering values of Re, λ, C_0, and M.

(v) With improving values of N_t, α_1, Ec, M, and N_b, the thermal boundary layer thickness and the temperature of the liquid are enlarged. And, they drop with varying Pr, Re, and C_0.

(vi) The concentration distribution portrays reducing response for increasing N_t, Pr, Le, Re, S, C_0, and N_b. However, it enhances gradually with raising α_2.

(vii) Microorganism profile shows mounting manner for all the parameters P_e, C_0, L_b, δ, Re, and S.

(viii) With mounting values of the variables L_b, Re, P_e, and C_0, the magnitude of Motile number depicts upward manner.

(ix) The local Sherwood number magnitude improves with L_e, N_b, and N_t. However, it reduces steadily for advanced values of Pr.

(x) The absolute values of surface drag force is uplifted with Re, λ, and C_0. Whilst, it drops mounting values of M, R_b, and Nr.

(xi) With amplifying N_t, α_1, Ec, M, N_b, and Pr, the absolute magnitude of heat transmission rate decays.

References

[1] Berman A S 1953 *J. Appl. Phys.* **24** 1232
[2] Abbas Z, Sajid M and Hayat T 2006 *Theor. Comput. Fluid Dyn.* **20** 229
[3] Ali N, Khan S U, Sajid M and Abbas Z 2016 *Nonlinear Engineering* **5** 73
[4] Aleem M, Asjad M I, Ahmadian A, Salimi M and Ferrara M 2020 *Eur. Phys. J. Plus* **135** 1
[5] Ali K, Ahmad A, Ahmad S, Nisar K S and Ahmad S 2023 *Waves in Random and Complex Media* 1
[6] Hamza M M, Abdulsalam S and Ahmad S K 2023 *Adv. Math. Phys.* 2023
[7] Sajid M, Iqbal S A, Naveed M and Abbas Z 2016 *J. Molecular Liquids* **222** 1115
[8] Abbas Z, Rafiq M and Naveed M 2018 *Journal of the Brazilian Society of Mechanical Sciences and Engineering* **40** 390
[9] Abbas Z, Imran M and Naveed M 2019 *Thermal Science-Part A* **23** 3379
[10] Abbasi A, Farooq W, Din E S M T, Khan S U, Khan M I, Guedri K, Elattar S, Waqas M and Galal A M 2022 *Micromachines* **13** 1415

[11] Naveed M, Imran M, Akhtar S, Abbas Z and Ullah S 2023 *Ricerche di Matematica* **72** 299
[12] Misra J C, Shit G C, Chandra S and Kundu P K 2011 *Journal of Engineering Mathematics* **69** 91
[13] Ali A and Asghar S 2014 *J. Aerospace Engineering* **27** 644
[14] Khan S U, Ali N, Sajid M and Hayat T 2019 *Proceedings of the National Academy of Sciences A: Physical Sciences* **89** 377
[15] Raghunatha K R and Vinod Y 2023 *Heat Transfer* **52** 5214
[16] Devi M P and Srinivas S 2023 *Nonlinear Analysis: Modelling and Control* **28** 1
[17] Naveed M, Imran M and Gul S 2023 *Advances in Mechanical Engineering* **15** 16878132231155823
[18] Imran M, Naveed M and Abbas Z 2023 *Advances in Mechanical Engineering* **15** 16878132231156742
[19] Imran M, Naveed M, Iftikhar B and Abbas Z 2023 *ZAMM Journal of Applied Mathematics and Mechanics/Zeitschrift für Angewandte Mathematik und Mechanik* e202200600
[20] Abbas Z, Imran M and Naveed M 2022 *Arabian Journal for Science and Engineering* **47** 16059
[21] Azam M, Khan W A and Nayak M K 2023 *Case Studies in Thermal Engineering* **49** 103250
[22] Naveed M 2023 *Chem. Phys. Lett.* 140682
[23] Sadighi S, Afshar H, Jabbari M and Ashtiani H A D 2023 *Case Studies in Thermal Engineering* **49** 103345
[24] Imran M, Abbas Z and Naveed M 2021 *Appl. Math. Mech.* **42** 1461
[25] Khan M R and Mao S 2023 *International Journal of Hydrogen Energy*
[26] Abbas N, Ali M, Shatanawi W and Mustafa Z 2023 *Alexandria Engineering Journal* **81** 101
[27] Faisal M, Ahmad I and Awan M A 2024 *Heat Transfer* **53** 646